RSC Advances

This article can be cited before page numbers have been issued, to do this please use: P. C. Faria-Tischer, C. Costa, I. Tozetti, L. H. Dall'Antonia and M. Vidotti, *RSC Adv.*, 2016, DOI: 10.1039/C5RA25332B.

ROYAL SOCIETY OF CHEMISTRY

www.rsc.org/advances

View Article Online
DOI: 10.1039/C5RA25332B

RSC Advances

ARTICLE

Structure and effects of gold nanoparticles into bacterial cellulose-polyaniline conductive membranes

Received 00th January 20xx,
Accepted 00th January 20xx

DOI: 10.1039/x0xx00000x

www.rsc.org/

Paula. C. S. Faria-Tischer [a,c]*, Carlos. A. R. Costa [b], Izadora Tozetti[c], Luiz H. Dall'Antonia[c] and Marcio Vidotti[a]

Abstract

Bacterial cellulose (BC) and poly(aniline) (PANI) composites were successfully synthesized by *in situ* polymerization of aniline by ammonium persulphate (APS) in the presence and absence of gold nanoparticles. The composites were fully characterized by different techniques such as SEM and AFM (morphology), Raman and FTIR spectroscopies (chemical structure), EFM (electrical conductivity), thermogravimetric analysis (thermal stabiliby), cyclic voltammetry (charge diffusion) and UV-Vis (optical properties). The surface roughness is higher in composites and the polymers interact each other by strong hydrogen bonds, providing high thermal stability in the BC/PANI composite. The phenazine structure was not present in this composite during synthesis; nevertheless, the local conductivity increased even further in the presence of AuNPs, inducing the interchain redox reactions leading the phenazine structures after electrochemical cycling. The electrical conductivity of composites in highly influenced by the APS in the polymerization step, as observed by EFM. Also, the presence of AuNPs leads to easier diffusional processes through the solid material, as observed by a more defined voltammetric waves.

Keywords: bacterial cellulose, poly(aniline), conductive polymers, biomaterial

Introduction

Cellulose is the most abundant biopolymer on earth and the structure of bacterial cellulose (BC) was described more than a century ago.[1,2] BC has been the most extensively investigated cellulose biomaterial for tissue engineering, and has been successfully applied to areas of biomedicine as topical wound dressings and drug delivery.[3] In particular, the interest in BC for medical applications is increasing due to its unique combination of mechanical properties (high wet strength), interconnected porosity, high purity, biocompatibility, and ability to absorb and hold large quantities of water. [4]

The most exciting applications of BC in the biomedical area is as wound dressing materials[5,6] artificial skin, vascular grafts, scaffolds for tissue engineering, artificial blood vessels, medical pads and dental implants. [7-10] Furthermore, BC has been utilized as biodegradable and biocompatible sensors. [11]

Polyaniline (PANI) exists in various structures that differs each other by the degree of the doping level, in which the electronic structure, optical properties and conductivity are depending on.[12] This conducting polymer has many interesting features, such as easy preparation and doping process, environmental stability, also presents potential use in different electrochemical based applications such as

[a] Grupo de Pesquisa em Macromoléculas e Interfaces, Department of Chemistry, Federal University of Parana, CxP 19032, CEP 81531-980 Curitiba, PR, Brazil. E-mail: paula.tischer@pq.cnpq.br
[b] National Nanotechnology Laboratory (LNNano), National Center for Energy and Materials (CNPEM), Campinas, São Paulo, Brazil 13083-970
[c] Laboratório de Eletroquímica e Materiais (LEMA), Department of Chemistry, CCE, State University of Londrina, PO Box 6001, 86051-990 Londrina, PR, Brazil.

View Article Online
DOI: 10.1039/C5RA25332B

electrochromic devices, sensors, corrosion protecting paint[13] and most recently biological research on PANI has also been investigated for the development of biosensors, neural probes, controlled drug delivery and tissue engineering applications.[14,15] It is known that the properties of conducting polymers in general depends on the structure and morphology which are related to the molecular ordering. The disorder in polymers and the conjugation defects limit the mobility of the charge carriers, thus affecting the electrical properties of the polymer.[16,17] The recent research efforts are to deal with the control and the enhancement of the bulk properties of PANI, mainly by formation of organized PANI chains in blends, composites and nanofibers.[18-21] However some important and obvious challenges can be highlighted as mechanical stability, tensile strength, toughness and biocompatibility.[22] Amongst eco-friendly nanofibrous materials, bacterial cellulose (BC) has recently been used to develop conductive polymer composites, especially because of its biocompatibility, low density, and noticeable properties of cellulose even in a hydrogel form. [20,23-25]

In order to diminish the intrinsic resistivity of conducting polymer and provide new features for these materials, composites of conducting polymers containing metal nanoparticles have been prepared. Amongst different metallic nanoparticles found in literature, the use of gold nanoparticles (AuNPs) stands out, due to their unique properties such as high chemical stability, biocompatibility and optical properties. [26-29]

The synthesis of gold-polyaniline composite materials was pioneered by Kang and co-workers.[30] Sarma et al. (2002)[31] reported a new method of synthesis of an Au nanoparticle-conductive polyaniline composite by using H_2O_2 both for reduction of $HAuCl_4$ and polymerization of aniline in the same aqueous medium, the composites showed electrical condutivity two orders of magnitude higher than the polymer itself.

By this way the objectives of this work are the synthesis and characterization of BC membranes modified by PANI and AuNPs aiming the formation of a new composite based on biological materials which presents high conductivity and electroactive properties. The morphology (SEM, AFM), thermal properties (TG, DTG), chemical structure (FTIR, UV-vis, Raman), electrical conductivity (EFM) and electrochemical behavior (CV) of the resulting composites were analyzed in detail. The results found herein indicate a potential development of electrochemically controlled drug delivery systems and biosensing electrodes.

Results and Discussion

Morphology and electrical properties

The photographs and SEM images of the native BC and modified BC samples are shown in the Figure 1. The network structure of the unmodified BC is made up of ribbon-shaped ultrafine nanofibers with width 100-140 nm, which forms three-dimensional porous network, this sample is visually almost transparent, as seen in Figure 1(a). After modification with PANI, the sample becomes dark green, due to the *in situ* polymerization of aniline by oxidation with APS. The PANI was deposited onto the nanofiber and the polymerization takes place preferentially on the cellulose fiber surface forming a coating layer, Figure 1(b). Even in the absence of reducing agent, AuNPs were synthesized in the BC sample, Figure 1(c), the immersion of BC into the $AuCl_4^-$ solution (yellowish) was enough to produce some gold nanostructures depicted by the change in the coloration of BC, becoming purple, which is a direct evidence of the presence of very small AuNPs[32,33], at this point, the presence of hydroxyl groups alongside the BC structure might be able to reduces small amount of $AuCl_4^-$ producing by this way the AuNPs, although in the respective SEM image is possible to observe few distinct spherical particles of around 100 nm.

In the Figure 1(d) is shown the micrograph of the BC/AuNPs/aniline sample, which was prepared by the BC/AuNPs sample after the immersion in aniline solution. It is possible to observe the greenish coloration, which is a direct evidence of the presence of PANI. The polymerization might occur due to the reaction between the reminiscent adsorbed $AuCl_4^-$ ions and the aniline monomer, in one-spot polymerization similar as vastly employed for the synthesis of AuNPs and PEDOT composites.[34,35,36] In the SEM image, more round particles are observed, which in principle, might be due to the polymerization of PANI with consequent formation of more AuNPs. There is no huge difference on the surface with the PANI adsorption, indicating that the amount of the conducting polymer is low, as the superficial concentration of $AuCl_4^-$ ions must be very low as well. The complete polymerization of PANI occurred after the addition of APS in the BC/AuNPs/aniline sample changing drastically the coloration to dark green producing the BC/AuNPs/PANI sample, as observed in the Figure 1(e), indicating that the polymerization was not complete by reacting unique with adsorbed $AuCl_4^-$ ions. In this sample, the surface is clearly different than the BC/PANI sample (Figure 1(b)), the PANI completely adsorbed onto the BC fibers, in this case, probably the first adsorption of both AuNPs and few segments of PANI might induce the polymerization. Round AuNPs are also observed in all over the surface.

View Article Online
DOI: 10.1039/C5RA25332B

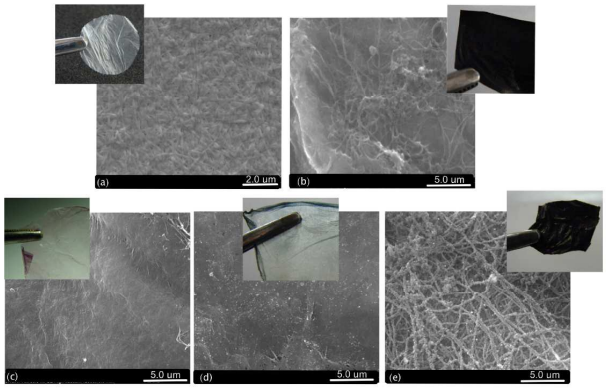

Figure 1. Representative digital photographs and SEM images of: (a) native bacterial cellulose (BC), (b) BC/PANI, (c) BC/AuNPs, (d) BC/AuNPs/aniline and (e) BC/AuNPs/PANI. The images were taken from different points of different samples.

Although the AuNPs influence on the PANI membrane were visually observed, the presence of the nanoparticles requires a further study of the materials on the other membranes. To do so, UV-Vis spectra were taken from each sample and the results are shown in Figure 2. The BC sample (Fig. 2a) shows no absorption band in the visible region, with an increase in absorption at the high energy transitions. The AuNPs signal can be visualized by the band centered in 540 nm (Fig. 2b), the SPB band in gold nanoparticles are very discussed in literature, this region corresponds to the signal of spheric AuNPs of about 50 nm in diameter.[37,38] The BC/AuNPs/aniline sample (Fig. 2c) presents absorption pattern along the visible region, corroborating the change in the coloration of the membrane, the spectrum also shows a wide band centered in 540 nm which can indicates the formation of more AuNPs and PANI as well. The intense band in 250 nm is related to the to the absorption of aniline monomers indicating that although PANI is present in this sample, the polymerization is not complete, due to the low amount ou $AuCl_4^-$ in the membrane, as commented earlier. In Figure 2d, the polymerization of more amount of PANI can be observed as an increase in the absorption in the visible region, corroborating the greenish coloration of the BC/PANI sample.

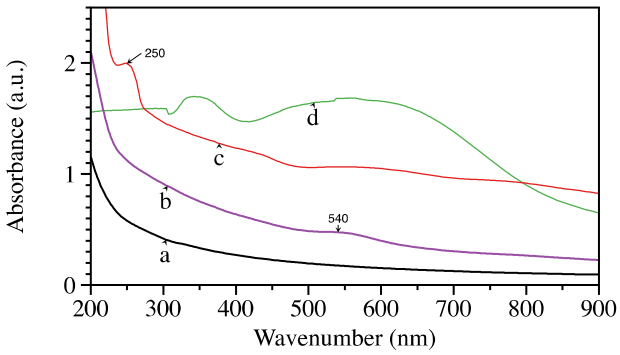

Figure 2. UV-Vis spectra taken from native (a) and the modified BC membranes, (b) BC/AuNPs, (c) BC/AuNPs/aniline and (d) BC/PANI.

The 3D topography images AFM clearly shows that the previous absorption of AuNPs changes the morphology of the bacterial cellulose membrane. In the surface of native BC the ribbons can be seen readily (Fig. 3a), the width was determined to be between 90-140 nm, values near those observed by SEM. The BC/PANI sample (Fig. 3b) showed a rougher surface, indicating the poly(aniline) polymerization. After immersion of the BC membrane in the $HAuCl_4$ solution the 3D-AFM shows that the surface has changed significantly (Fig. 3c) and the ribbons cannot be seen anymore. The same effect is observed in the BC/AuNPs/aniline and BC/AuNPs/PANI sample (Fig. 3d and 3e) and some connected PANI particles appear on the BC nanofibers as previously seen in the SEM image. After addition of APS, it has appeared a large number of particles uniformly dispersing on the whole surface of the BC film; no fiber was observed. The surface morphology and surface characteristics are important factors in the interfacial interactions, and these differences can be proven by changes in roughness. It is possible to observe that the surface roughness changed drastically with the membrane modifications. The roughness values of the composite films (estimated as root mean square, RMS) were obtained by using height distribution analysis.

Native bacterial cellulose presents smoother surface (RMS = 33.4 nm) and this value increased with PANI deposition (RMS = 87.2 nm). The presence of AuNPs increased the roughness (RMS = 75.2 nm) and by adding aniline, the roughness increased even further (RMS = 91.6 nm) as well after PANI polymerization (RMS =143.2 nm). Topographical features as showed herein can be used to tune the specific application of the conductive composite, e.g. in tissue engineering, where has been demonstrated that the surface roughness of scaffolds affects cell behavior, including cell attachment, proliferation and differentiation.[39,40] Gomez et al. synthesized PPy (polypyrrole) microchannels electro-chemically to fabricate electroconductive, topographical substrates for neural interfacing and found that PPy microchannels facilitated axonal establishment of rat embryonic hippocampal neurons.[41]

View Article Online
DOI: 10.1039/C5RA25332B

RSC Advances

ARTICLE

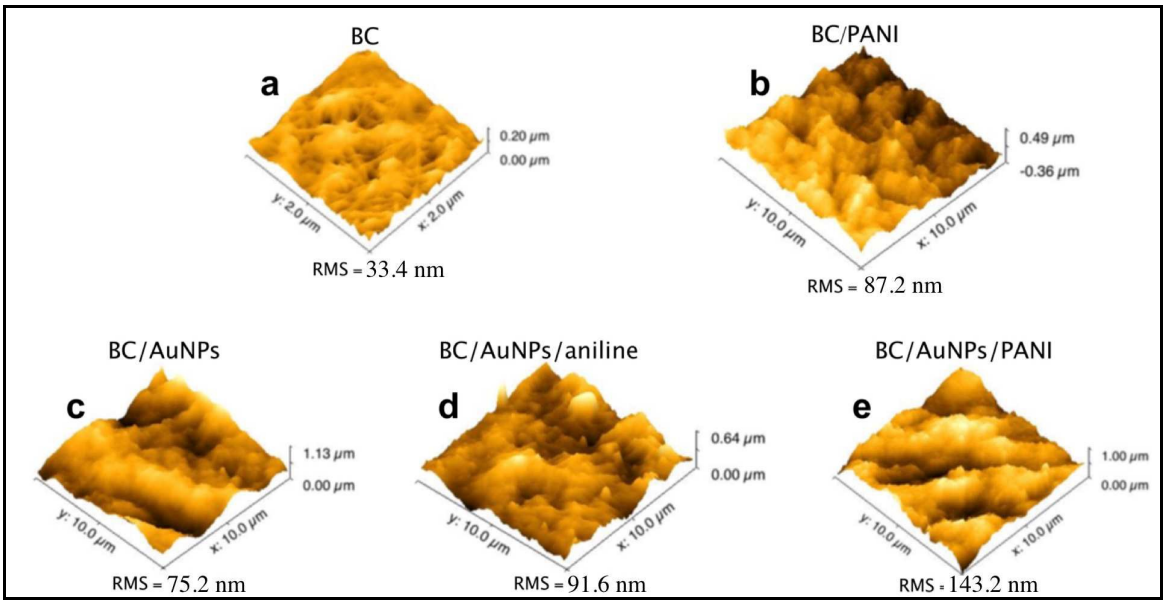

Figure 3. 3D-AFM topography of BC and composite films.

The study of the electrical properties of conductive membranes was realized by the capacitance coupling analysis. Capacitance gradient (dC/dZ) measurements can be performed in the intermittent contact regime in different environments; this methodology provides the measurement of the capacitance gradient with nanometer-scale spatial resolution.[42] The dC/dz information can be used to estimate the difference in the capacitance and therefore the difference in dielectric constant along the sample areas.[43] In the figure 4a, comparing the topographic image of bacterial cellulose with the corresponding map dC/dz (Fig. 4b) it can be seen that where the cellulose fibers are present there is low charge mobility. In regions where there are depressions between the fibers can be noticed greater charge mobility (presumably due to the residual presence of solvated ions in these regions).

After the adsorption of $AuCl_4^-$ followed by the reduction of few sites of AuNPs, the presence of the later ones in the bacterial cellulose fibers, provided greater uniformity of charge mobility as well as increased average mobility (Fig. 4f). The increase of conductivity with AuNPs deposition on BC contributes for the observation that the structure of cellulose can act as a reducing and stabilizing agent of these nanoparticles, preventing aggregation, as observed with another biopolymer, e.g. Arabic gum[33], once in the nanometric scale the physical and chemical properties depends mainly on the interfacial characteristics.[44]

The Fig. 4g shows the topographic image of the membrane with AuNPs and aniline. In the corresponding map dC/dz (Fig 4h) is easily observed regions with different electric charge mobility (darker with low mobility and brighter domains with high mobility). After addition of APS, and consequent PANI formation, (Fig. 4j) the charge mobility is more uniform. We attribute this to the increase of electrical conductivity by the polymerization of regions rich in aniline that has not been previously polymerized by $AuCl_4^-$, as discussed in the UV-Vis results. The dC/dz maps of membranes, which the APS was used as oxidant agent of aniline (Fig. 4d and 4j) shows that the presence of AuNPs (Fig. 4j) does not change significantly the profile of electrical mobility distribution. This suggests that electric mobility is mainly determined by PANI.

View Article Online
DOI: 10.1039/C5RA25332B

RSC Advances

ARTICLE

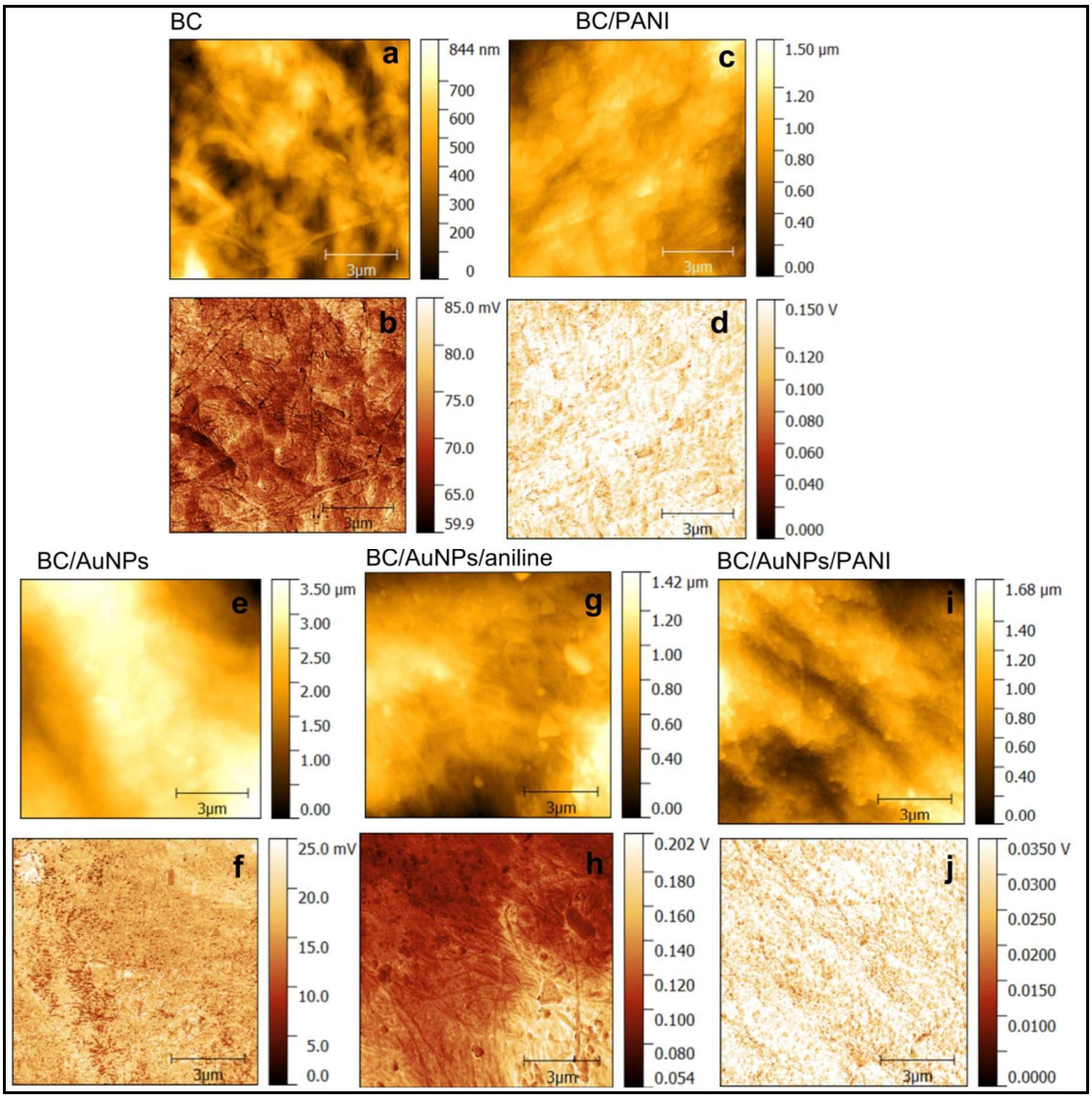

Figure 4. Topography AFM (a,c,e,g,i) and respective dC/dz maps (b, d,f,h,j) of native bacterial cellulose and modified membranes.

Chemical Interaction

The adsorption of PANI and AuNPs on the BC membranes was further characterized by vibrational spectroscopy. In Figure 5 are shown the ATR-FTIR spectra of the samples. The spectrum of BC shows the characteristic behavior, the main bands can be detailed as follows. The wide band at around 3359 cm^{-1} is assigned to the OH stretch[20], the 1427 cm^{-1} band represents CH_2 scissoring motion; the 895 cm^{-1} band indicates the vibrational mode involving C_1 and four atoms attached to it, which is characteristic of β-anomers or β-linked glucose polymers[45]; the 1370 cm^{-1} band is for C–H bending mode, and the 2917 cm^{-1} band represents C–H and CH_2 stretching.[46]

View Article Online
DOI: 10.1039/C5RA25332B

RSC Advances

ARTICLE

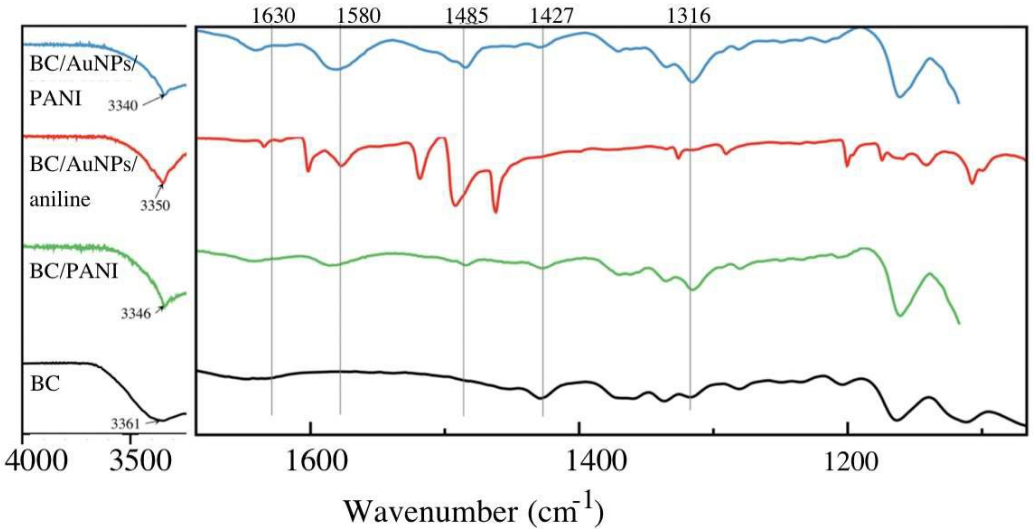

Figure 5. FTIR spectra of the native and modified BC membranes.

The FTIR spectra of pure PANI is vastly found in literature and by comparing these works with our results, some important differences were found. The most interesting one is the shifting of the N-H band. In pure PANI, this band can be found at about 3470 cm^{-1} [47-49] but in our results, this band is seen at around 3350 cm^{-1}. This shifting is well estabilished in literature as being of consequence of strong hydrogen interaction[49,50] and commonly seen in other polyssacharides/PANI composites.[76,52-54] By this way, the same effect can be observed herein the BC modified membranes where the lateral OH groups are strongly interacting with the NH sites of PANI. This strong interaction can also be observed in the band in 1316 cm^{-1}, corresponding to C–H stretching of CH_2 in BC.[55] When PANI is present in higher amount, this band increases its intensity. The bands in 1580 cm^{-1} and 1485 cm^{-1} are normally studied together and are assigned to the presence of quinoid and benzenoid ring, respectively.[56-58] Some authors correlate these bands to find out the degree of doping of PANI and in our findings these bands present at almost the same intensity in the BC/AuNPs/PANI and BC/PANI samples indicating the high doping level of PANI. Nevertheless in the BC/AuNPs/aniline sample, the benzenoid signal is seen as a shoulder with higher intensity if compared with the quinoid band. Also, a strong band is observed at around 1490 cm^{-1}, probably due to the presence of the aniline monomer, as seen in the EFM and UV-Vis experiments. Regarding this sample, some sharp bands are observed in around 1600, 1519 and 1462 cm^{-1} probably due to the presence of unreacted $AuCl_4^-$. By this way, the FTIR corroborates the main results described so far regarding the incomplete aniline polymerization in the BC/AuNPs/aniline sample and the presence of conducting PANI in a good doping level. Another interesting point which is highly desirable, aiming a high stable material was observed in terms of the strong hydrogen bonding between PANI and BC. In order to verify this issue thermogravimetric experiments were conducted.

Thermogravimetric Analyses

In Figure 6 are shown the TG curves of the native BC and the composites. Usually it is reported in the literature that polyaniline has three main stages of mass loss associated with adsorbed water loss, elimination of doping ions of the polymer backbone and finally to the polymer degradation.[59,60] During the initial stage at 30–100 °C, the moisture present in the native BC and in the composites evaporates. In order to analyze the thermal stability of the composites it was found the $T_{10\%}$ (temperature the degradation of 10% of the material)[61]. It was observed that the stability of the composite is near to BC ($T_{10\%}$ BC = 276.8°C, and BC/PANI = 271.5°C) showing that the composite material is stabilized by strong hydrogen bonds. In the presence of AuNPs the thermal stabilized was reduced, as observed in the samples BC/AuNPs/aniline and BC/AuNPs/PANI ($T_{10\%}$: 117.9°C and 187.4°C, respectively). Apparently the presence of a large amount of PANI provides a further stabilization of the

View Article Online
DOI: 10.1039/C5RA25332B

composite. In the DTG curves (Fig.6(b)), it is possible to observe an event in the sample BC/AunPs/aniline at 147°C, it is probably related to the removal of adsorbed aniline monomers in the membrane. In the composites containing AuNPs a small event (also indicated by the arrow) is present, this could be attributed to the degradation of phenazine structures, derived from the cross-linking of PANI chains[62].To further investigate this issue, Raman experiments were performed and will be shown ahead. The further decomposition above this temperature is mainly due to chemical oxidative degradation of PANI.[63]

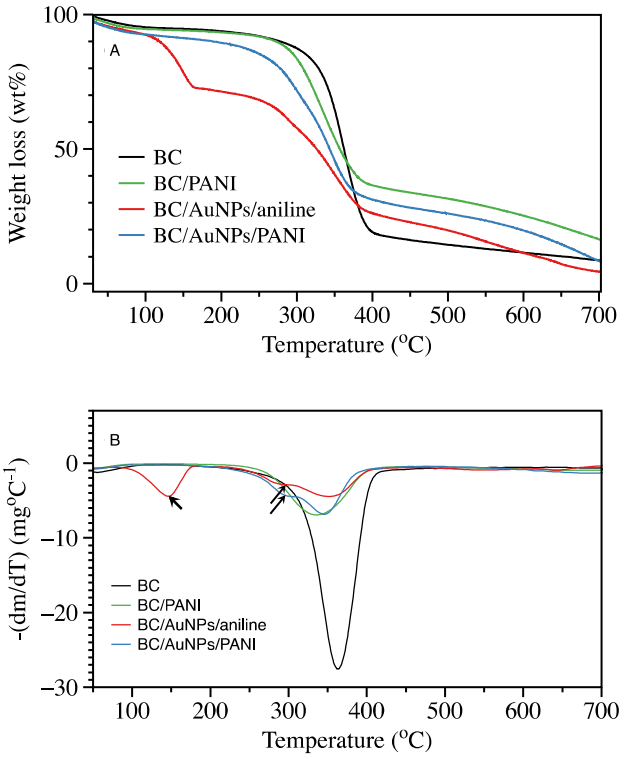

Figure 6. TGA (A) and DTG (B) curves for native bacterial cellulose (BC) and the composites.

Electroactive Properties and influence of the AuNPs

Regardless the intended application of the BC membranes, it is important to verify the electroactive properties of the PANI and the influence of AuNPs in this issue. To do so, Raman and voltammetric experiments were performed. Raman experiments are very important, as due to the resonant effect found for conducting polymers[64,65], important features could be evidenced on the PANI chain avoiding any spectroscopic signal from the BC, giving by this way a complete vibrational characterization of PANI.

In Figure 7 are shown the Raman spectra taken from the BC/PANI, BC/AuNPs/PANI and pure PANI samples. The modified BC membranes have a distinct behavior if compared with pure PANI. The most intense band, centered in 1166 cm^{-1} is found in all samples and is related to the in plane C-H bending.[66,67] The band in 1336 cm^{-1} is found with high intensity for the BC/PANI and BC/AuNPs/PANI samples and it is assigned to the in plane C-N^{+} stretch, characteristic of high doped PANI, this band appears as a discrete contribution in the pure PANI sample. The same behavior is found for the 1514 cm^{-1} band, which is wide and has a moderate intensity in the membranes and in the pure PANI spectra appears as a shoulder with low intensity. This band is assigned to in plane N-H bending and the behavior described is direct evidence of the hydrogen bonding of the surrounding. The 1594 cm^{-1} band is assigned to C-C stretch of intermediate quinoid and benzenoid rings[68] and the 1645 cm^{-1} band present in pure PANI sample is assigned to the C-C in the benzenoid structure[69], corroborating the low degree of doping of this sample compared with the other ones.

The low frequency bands at 420 and 520 cm^{-1} are found in all samples and are related to the out-of-plane torsion and in plane amine deformation.[70,71] The bands in 577 cm^{-1} is assigned to the presence of phenazine structures derived from the cross-linking of PANI chains.[66,67,70,71] This is a very common band found in many different works that synthesize PANI by aqueous chemical reaction and this structure is not found in the BC/PANI sample. This fact is probably due to the strong interaction between PANI and BC by means of the hydrogen bonds. This interaction might protect the amine sites from parallel reaction with other PANI chain. On the other hand, on the presence of AuNPs, this band is found. As reported previously[31], the AuNPs adsorbed in PANI structure intensifies the charge transfer from polyaniline to the gold nanoparticles. So, the redox reactions are facilitated by the metallic nanoparticle, allowing by this way the redox reaction between adjacent PANI chains, leading to the phenazine structures. The presence of AuNPs also leads to the 611 cm^{-1} band which is related to the in plane benzene deformation[70,71] not seen in the BC/PANI spectrum, which is quite feasible by adding a metallic nanoparticle into the polymeric chain.

View Article Online
DOI: 10.1039/C5RA25332B

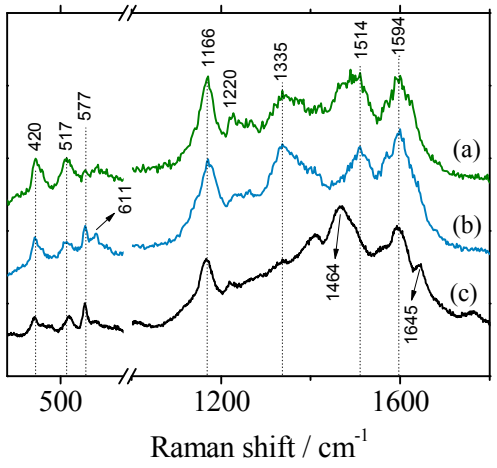

Figure 7. Raman spectra of the (a) BC/PANI, (b) BC/AuNPs/PANI and (c) PANI, λ_0 = 632.8 nm.

Finally, modified electrodes were tested in order to verify the voltammetric behavior of the BC membranes. In Figure 8 are shown the cyclic voltammograms of the BC/PANI and BC/AuNPs/PANI modified electrodes. The PANI electrochemical behavior is vastly found in literature and comprises of two distinct processes: the first one at about 0.2 V is the first oxidation reaction, leading the leucoemeraldine base to the emeraldine salt, the second one at 0.7 V is the second oxidation step converting the salt emeraldine to pernigraniline.[72,73] In the modified electrodes showed herein, the voltammograms present a slight resistive behavior, due to the insulate cellulose membrane but the redox processes of PANI are seen at the respective traditional potentials, anyway in the presence of AuNPs, two differences can be pointed out. The first one is about the shape of the redox wave being clearly more defined, which is a direct evidence of easy diffusional processes through the solid material. This result is in good agreement with the AFM and SEM images where this material presented more roughness and a disordered morphology. The second point is the third redox reactions at about 0.5 V, this region is described in literature to the phenazine structures.[67] This result is in perfect agreement with the Raman and TGA results and the appearing of these structures can be linked to the presence of AuNPs, which increases the conductivity of a specific region being by this way more suitable for electron exchange between the PANI chains, as observed experimentally.

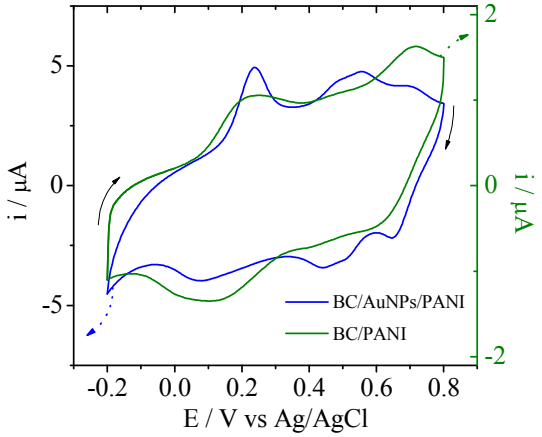

Figure 8. Cyclic voltammograms of the BC/PANI (green line) and BC/AuNPs/PANI (blue line) composites films in aqueous H_2SO_4 (0.05 mol.L^{-1}) in potential range (-0.2 a 0.8 V) with a scan rate of 50 mVs^{-1}.

Conclusions

In the present work, we have demonstrated that conductive composites of PANI and BC have been successfully synthesized by *in situ* by oxidative polymerization of aniline by APS in the presence or absence of gold nanoparticles. The PANI was deposited onto the surface of BC increasing the roughness of the membranes. The presence of gold nanoparticles provides distinct differences in the chemical structure of PANI and also in voltammetric profile. The AuNPs were confirmed by UV-Vis and EFM, the later one indicated the increase of the electrical conductivity and charge distribution over the BC membrane. FTIR spectra showed that PANI is linked in BC by strong hydrogen bonding, which provided a good thermal stability of the PANI composites and also avoids the formation of phenazine structures, as observed by Raman. Nevertheless, the presence of AuNPs has increased the local electrochemical activity, leading to the formation of the phenazine structures, also confirmed by Raman and TGA experiments. The voltammograms presented the redox processes of PANI at the respective traditional potentials, and the presence of AuNPs enhanced the diffusional processes through the solid material. It was also observed the redox behavior of phenanize structures in the BC/AuNPs/PANI modified electrode.

Experimental section

H_2SO_4 89% (Merck), ammonium persulphate (APS) (Merck), were used as received. Aniline (Aldrich) was distilled under low pressure before use. $HAuCl_4$ solution was obtained from Sigma. All solutions were prepared using Milli-Q water. The synthesized membranes were adsorbed onto ITO electrodes (sheet resistance <15 Ω/sq) electrodes were purchased from Delta Technologies by using a conductive

View Article Online
DOI: 10.1039/C5RA25332B

carbon tape.

Microorganism, Culture Media, and Growth Conditions. The bacterial strain *Gluconacetobacter xylinum* was grown in a glucose medium based on the Hestrin-Schramm's medium culture.[74] The inoculum and fermentation process was realized as described by Faria-Tischer et al. 2010.[75]

Treatment of Bacterial Cellulose. The bacterial cellulose (BC) membrane formed was removed, washed in deionized water and purified by immersion in an aqueous solution of 0.1 M NaOH for one day. The NaOH was removed by washed the membranes repeatedly with deionized water until neutral pH and the membranes were dried in stove at 50°C.[75]

Preparation of the conductive membranes without gold (BC/PANI). Dried BC membranes were soaked in an acid solution containing 0.5 mL aniline, 32 mL Milli-Q water and 4 mL of HCl (1.7 mol L^{-1}), as reported previously by Quintanilha, 2014.[76] After one hour the membranes were washed with Milli-Q water and dried in stove at 50°C and let it rest in a Petri dish. The polymerization of aniline was performed by adding 100 µL of APS solution (0.4 mol L^{-1}) on the sample for 15 minutes, after this, the samples were washed and dried in stove under 50°C. The sample prepared with this methodology was named as BC/PANI.

Preparation of the conductive membranes with gold (BC/AuNPs/aniline and BC/AuNPs/PANI). The second methodology consists in a first adsorption of AuNPs onto the BC membrane prior the PANI synthesis. By this way, the BC membranes were immersed in $HAuCl_4$ solution (1 mmol L^{-1}) during 24 hours, achieving the BC/AuNPs sample. This one was placed in an aniline solution for 1 hour, producing the BC/AuNPs/aniline sample. The membrane prepared by this way was cutted in pieces of 1.7 cm^2 and 100 µL of APS was pipetted over the membrane, covering the entire surface. The polymerization occurred during 15 minutes, finally producing the BC/AuNPs/PANI sample. In between each procedure, as done for the first methodology, the modified BCs were washed in water and dried in stove under 50°C. Both methodologies are resumed in a Scheme 1.

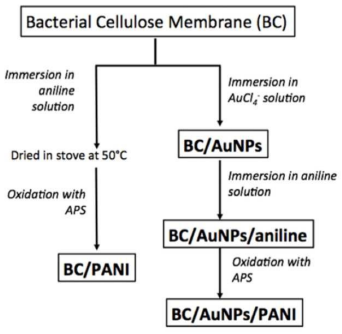

Scheme 1. Schematic representation of the BC modified samples synthesized in this work.

Electrochemical and spectroscopic experiments. The electrochemical experiments were performed in an Autolab PGSTAT 30 potentiostat in a three electrode conventional electrochemical cell, using Pt foil and $Ag/AgCl/Cl^-_{sat}$ as counter and reference electrodes respectively. The ITO-BC modified electrodes were tested using H_2SO_4 0.05 mol L^{-1} electrolyte. Attenuated total reflection Fourier-transformed infrared spectroscopy (ATR-FTIR) of PANI and BC samples were recorded by using a FT-IR Bommen MB-100 in transmission mode over the 4000–400 cm^{-1} range under a N_2 atmosphere. The spectra were collected with a resolution of 1 cm^{-1} and a total of 8 scans per sample. Raman measurements were done by using a Witec Alpha 300R equipment, operating ata wavelength of 632.8 nm, with a resolution of 0.02 cm^{-1}.

Thermogravimetric analyses. Thermal gravimetric (TG) curves were performed on Shimadzu TGA-50. Samples were heated in open alumina pans from 30°C to 800°C, under a nitrogen atmosphere, at a heating rate of 10°C/min under nitrogen flow.

Ultraviolet-visible analysis. UV-Vis analysis of the membranes native and modified were carried out in a Shimadzu UV-2600 UV-visible spectrophotometer equipped with a film holder (P/N 204-58909) direct in the film in the range 200 – 800 nm.

Scanning Electron Microscopy (SEM) Analysis. The morphologies of the BC samples were analyzed by using a FEI Quanta 200 microscope (Oregon, USA) in State University of Londrina (UEL). Membranes pieces were mounted on the bronze stubs using double-sided tape.

Atomic Force Microscopy (AFM) and Capacitance Coupling (dC/dz). Topography images and capacitance gradient (dC/dz) maps of the native bacterial cellulose and composites were obtained in a FlexAFM Atomic Force Microscope (Nanosurf), using an PPP-EFM (NanoSensors) Si probe PtIr coated, with spring constant of 2.8 N m^{-1} and resonance frequency within 75 kHz. The capacitance coupling (d*C*/d*z*) analysis was realized to study the electrical properties of conductive membranes.[77]

In a scanning, the EFM probe and sample surface are maintained at close proximity, in intermittent contact mode slightly below the frequency of resonance. When a voltage difference ΔV occurs between the EFM probe and sample surface, the electrostatic force F_e can be written as:

$$F_e = -\frac{1}{2}\Delta V^2 \frac{\partial C_{(z)}}{\partial z}$$

When $\frac{\partial C_{(z)}}{\partial z}$ is the capacitance gradient, or capacitance coupling, between EFM probe and sample.

View Article Online
DOI: 10.1039/C5RA25332B

In the electric mode experiments, AC and DC signals are applied in addition to the probe, resulting in an electrostatic force F_e:

$$F_e = -\frac{1}{2}\frac{\partial C_{(z)}}{\partial z}\left[V_{dC} - V_{CPD} + V_{AC}\sin(\omega t)\right]^2$$

When V_{CPD} is the contact potential difference and ω is the frequency of V_{AC} signal.

This equation can be decomposed into three contributions of forces, dependent on the frequencies 0, ω and 2ω:

$$F_{dc} = -\frac{1}{2}\frac{\partial C_{(z)}}{\partial z}\left[\frac{1}{2}(V_{dC} - V_{CPD})^2\right]$$

$$F_{\omega} = -\frac{\partial C_{(z)}}{\partial z}(V_{dC} - V_{CPD})V_{AC}\left[\sin(\omega t)\right]$$

$$F_{2\omega} = \frac{1}{4}\frac{\partial C_{(z)}}{\partial z}V_{AC}^2\left[\cos(2\omega t) - 1\right]$$

In the same pass in with the topography is acquired, V_{AC} signal at ω frequency is applied to the probe and Kelvin Force feedback is used to nullify the difference $V_{dC} - V_{CPD}$ and consequently the forces F_{dc} and F_{ω}. A lock-in amplifier is used for detecting the signal at 2ω (second harmonic of the electrical modulation), proportional to $F_{2\omega}$, this presenting a simple linear dependence of $\frac{\partial C_{(z)}}{\partial z}$.

Acknowledgments

The authors wish to thank the Laboratory of Microscopy and Microanalysis (LMEM) and to the Spectroscopy Laboratory (LABSPEC) in the Universidade Estadual de Londrina (UEL) for the FTIR and UV-Vis analyses. We would like to thank to Dr. Gizilene Carvalho for discussion about TG results. Also, thanks for Conselho Nacional de Desenvolvimento Científíco e Tecnológico (CNPq/Brazil) (grant 158705/2014-9) for financial support.

References

1 D.J. Gardner, G.S. Oporto, R. Mills, M.A.S. Azizi Samir, *J. Adhes. Sci. Technol,* 2008, **22**, 545.
2 A.J. Brown, *J. Chem. Soc*, 1886, **49**, 172.
3 J.M. Dugan, J.E. Gough, S.J. Eichhorn, *Nanomedicine*, 2013, **8**, 287.
4 M. Iguchi, S. Yamanaka, A. Budhiono, *Journal of Materials Science*, 2000, **35**, 261.
5 D. Ciechanska, *Fibres and Textiles in Eastern Europe*, 2004, **12**, 69.
6 W. Czaja, A. Krystynowicz, S. Bielecki, R.M. Brown, *Biomaterials*, 2006, **27**, 145.
7 W. Czaja, D.J. Young, M. Kawechi, R.M. Brown, *Biomacromolecules*, 2007, **8**, 1.
8 D. Klemm, D. Schumann, U. Udhardt, S. Marsch, *Prog. Polym. Sci*, 2001, **26**, 1561.
9 O. Shezad, S. Khan, T. Khan, J.K. Park, *Korean J Chem Eng*, 2009, **26**, 1689.
10 W.K. Wan, J.L. Hutter, L. Millon, G. Guhados, *ACS Symposium Series*, 2006, **938**, 221.
11 J.H. Jeon, I.K. Oh, C.D. Kee, S.J. Kim, *Sensor Actuat B-Chem*, 2010, **146**, 307.
12 W.S. Huang, A.G. MacDiarmid, *Polymer* 1993, **34**, 1833.
13 J. Liu, Y. Lin, L. Liang, J. A. Voigt, D. L. Huber, Z. R. Tian, E. Coker, B. Mckenzie, M. J. Mcdermott, *Chemistry*, 2003, **9**, 604.
14 X. Liu, K.J. Gilmore, S.E. Moulton, G. G. Wallace, *J Neural Eng* 2009, **6**, 1.
15 P. Humpolicek, V. Kasparkova, P. Saha, J. Stejskal, *Synth. Met*, 2012, **162**, 722.
16 A. G. MacDiarmid, A. J. Epstein, *Synth. Met*, 1995, **69**, 85.
17 K. Lee, A. J. Heeger, Y. Cao, *Synth. Met*, 1995, **72**, 25.
18 A. G. MacDiarmid, A. J. Epstein, *Faraday Div. of the Chemical Society*, 1989, **88**, 317.
19 A. G. MacDiarmid, A. J. Epstein, In: *Conducting polymers, emerging technologies*, Eds. Technical Insights, New Jersey 1989; p27.
20 D. Müller, C. R. Rambo, D. O. S. Recouvreux, L. M. Porto, G. M. O. Barra, *Synth. Met*, 2001, **161**, 106.
21 L. F. Marchesi, S. C. Jacumasso, R. C. Quintanilha, H. Winnischofer, M. Vidotti, *Electrochim. Acta*, 2015, **174**, 864.
22 A. Guiseppi-Elie, *Biomaterials*, 2010, **31**, 2701.
23 J. A. Marins, B.G. Soares, K. Dahmouche, S. J. L. Ribeiro, H. Barud, D. Bonemer, *Cellulose*, 2011, **18**, 1285.
24 W. Hu, S. Chen, Z. Yang, L. Liu, H. Wang, *J. Phys. Chem. B*, 2011, **115**, 8453.
25 B-H. Lee, H-J. Kim, H-S. Yang, *Current Applied Physics*, 2012, **12**, 75.
26 A. Kyrychenko, G. V. Karpushina, D. Svechkarev, D. Kolodezny, S. I. Bogatyrenko, A. P. Kryshtal, A. O. Doroshenko, *J. Phys. Chem*, 2012, **116**, 21059.
27 M. Alvaro, C. Aprile, B. Ferrer, F. Sastre, H.

View Article Online
DOI: 10.1039/C5RA25332B

García, *Dalton Trans*, 2009, **36**, 7437.
28 M-C. Daniel, D. Astruc, *Chem Rev*, 2004, **104**, 293.
29 J. C. S. Costa, R. A. Ando, A. C. Sant'Ana, L. M. Rossi, P. S. Santos, M. L. A. Temperini, P. Corio, *Physical Chemistry Chemical Physics,* 2009, **11**, 7491.
30 E. T. Kang, K. G. Neoh, K. L. Tan, *Prog. Polym. Sci*, 1998, **23**, 277.
31 T. K. Sarma, D. Chowdhury, A. Paul, A. Chattopadhyay, *Chem. Commun*, 2002, **10**, 1048.
32 X. Wu, C. Lu, Z. Zhou, G. Yuan, R. Xiong, X. Zhang, *Environ. Sci. Nano*, 2014, **1**, 71.
33 C. Wu, D. Chen, *Gold Bull* 2010, **43**, 234.
34 I. Rocha, E. Lucht, I. C. Riegel-Vidotti, M. Vidotti, E. S. Orth, *J. Phys. Chem. C*, 2014, **118**, 25756.
35 S. S. Kumar, C. S. Kumar, J. Mathiyarasu, K. L. Phani, *Langmuir*, 2007, **23**, 3401.
36 T. Augusto, É. T. Neto, Â. A. T. Neto, R. Vichessi, M. Vidotti, S. C. Torresi, *Sol Energ Mat Sol C*, 2013, **118**, 72.
37 D. E. Astruc, M. C. Daniel, *Chem. Rev*, 2004, **104**, 293.
38 S. Link, M. A. El-Sayed, *Int Rev Phys Chem*, 2000, **19**, 409.
39 U. Meyer, D. H. Szulczewski, K. Moller, H. Heide, D. B. Jones, *Cell Mater*, 1993, **3**, 129.
40 A. Naji, M. F. Harmand, *J Biomed Mater Res*, 1990, **24**, 861.
41 N. Gomez, J. Y. Lee, J. D. Nickels, C. E. Schmidt, *Adv Funct Mater*, 2007, **17**, 1645.
42 S. Magonov, J. Alexander, J. Beilstein *Nanotechnol*, 2011, **2**, 15.
43 E. S. Ferreira, E. M. Lanzoni, C. A.R. Costa, C. Deneke, J. S. Bernardes, F. Galembeck, *ACS Appl. Mater. Interfaces*, 2015, **7**, 18750.
44 A. Muller, Nanomaterials – An Introduction In: *The Chemistry of Nanomaterials: Synthesis, Properties and Applications*, 2 vols. Eds: Rao, C.N.R.; Muller, A.; Cheetham, A.K. Willey-VCH, Weinhein, 2004, p5.
45 M. L. Nelson, R. T. O'Connor, *J. Appl. Polym. Sci*, 1964b, **8**, 1325.
46 M. L. Nelson, R. T. O'Connor, *J. Appl. Polym. Sci*, 1964a, **8**,1311.
47 Z. Ping, G. E. Nauer, H. Neugebauer, J. Theiner, *J. Electroanal. Chem*, 1997, **420**, 301.
48 N. V. Blinova, J. Stejskal, M. Trchová, J. Prokes, *Polymer*, 2006, **47**, 42.
49 A. Y. Arasi, J. J. L. Jeyakumari, B. Sundaresanb, V. Dhanalakshmi, R. Anbarasand, *Spectroc. Acta A*, 2009, **74**, 1229.
50 T. Steiner, *Angew. Chem. Int*. Ed. 2002, **41**, 48.
51 W. B. Stockton, M. F. Rubner, *Macromolecules*, 1997, **30**, 2717.
52 C. Eiras, I. N. G. Passos, A. C. F. De Brito, J. R. Jr. Dos Santos, V. Zucolotto, O. N. Jr. Oliveira, I. L. Kitagawa, C. J. L. Constantino, H. N. Da Cunha, *Quim. Nova*, 2007, **30**, 1158.
53 D. Cheng, H. Xia, H. S. O. Chan, *J. Nanosci. Nanotechnol*, 2005, **5**, 474.
54 A. Tiwari, S. K. Shukla, *E-xpress Polym. Lett*, 2009, **3**, 553.
55 R. L. Oliveira, J. G. Vieira , H. S. Barud, R. M. N. Assunção, G. R. Filho, S. J. L. Ribeiro, Y. Messadeqq, *J. Braz. Chem. Soc*, 2015, **26**, 1861.
56 N. V. Blinova, J. Stejskal, M. Trchová, J. Prokes, M. Omastová, *Eur. Polym. J*, 2007, **43** 2331.
57 L. Brozova, P. Holler, J. Kovarova, J. Stejskal, M. Trchová, *Polym. Degrad. Stab*, 2008, **93** 592.
58 M. Trchová, J. Stejskal, *Pure Appl. Chem*, 2011, **83**, 1803.
59 C. Chen, *J Polym Res*, 2002, **9**, 195.
60 H. S. O. Ghan, L. M. Gan, T. S. A. Hor, S. H. Seow, L. H. Zhang, *Thermochim Acta,* 1993, **225**, 75.
61 J. Lenza, M. Sozanska, H. Rydarowski, *in*: Reactions and Mechanisms in Thermal Analysis of Advanced Materials, ed. A. Tiwari, B. Raj Scrivener Publishing, Wiley, 2015, 4, 85-100.
62 J. Laska, J. Widlarz, *Polymer,* 2005, **46**, 1485.
63 Z. L. Mo, Z. L. Zhao, H. Chen, G. P. Niu, H. F. Shi, *Carbohydr. Polym*, 2009, **75**, 660.
64 W. J. Kiefer, *Raman Spect,* 2007, *38*, 1538-1553
65 Y. Furukawa, *J. Phys. Chem*, 1996, **100**, 15644.
66 G. Louarn, M. Lapkowski, S. Quillard, A. Pron, J. *P. Buisson, S. Lefrant, 1996. J. Phys. Chem, 1996,* **100**, 6998.
67 J. E. P. Da Silva, M. L. A. Temperini, S. I. De Torresi, *J. Braz. Chem. Soc*, 2005, **16**, 322.
68 I. Sedenkova, M. Trchova, J. Stejskal, *Polym. Degrad. Stab*, 2008, **93**, 2147.
69 T. Lindfors, A. Ivaska, *J. Electroanal. Chem*, 2005, **580**, 320.
70 M. Cochet, G. Louarn, S. Quillard, M. I. Boyer, J. P. Buisson, S. Lefrant, *J. Raman Spectrosc*, 2000, **31**, 1029.
71 M. Trchová, Z. Moravkova, J. Stejskal, I. Šeděnková, *Chem. Pap*, 2012, **66**, 415.
72 E. M. Genies, C. Tsintavis, *J. Electroanal. Chem*, 1985, **195,** 109.
73 H. Varela, S. L. D. A. Maranhão, R. M. Q. Mello, E. A. Ticianelli, R. M. Torresi, *Synth. Metals*, 2001, **122**, 321.
74 S. Hestrin, M. Schramm, *Biochem. J*, 1954, **58**, 345.
75 P.C.S. Faria-Tischer, M. R. Sierakowski, H. Jr. Westfahl, C. A. Tischer, *Biomacromolecules*,

View Article Online
DOI: 10.1039/C5RA25332B

2010, **11**, 1217.

76 R. C. Quintanilha, E. S. Orth, A. Grein-Iankovski, I. C. Riegel-Vidotti, M. Vidotti, *J Colloid Interface Sci*, 2014, **434**, 18.

77 F. C. Salomão, E. M. Lanzoni, C. A. Costa, C. Deneke, E. B. Barros, *Langmuir*, 2015, **31**, 11339.

Conductive films

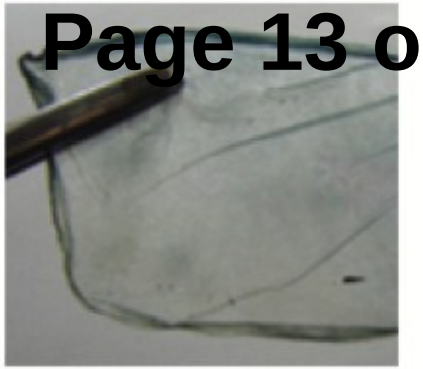

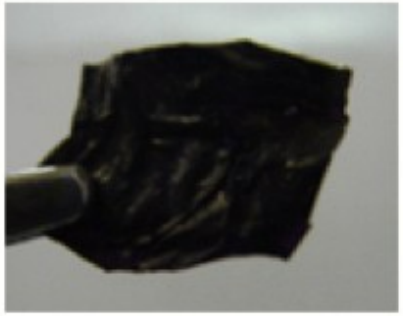

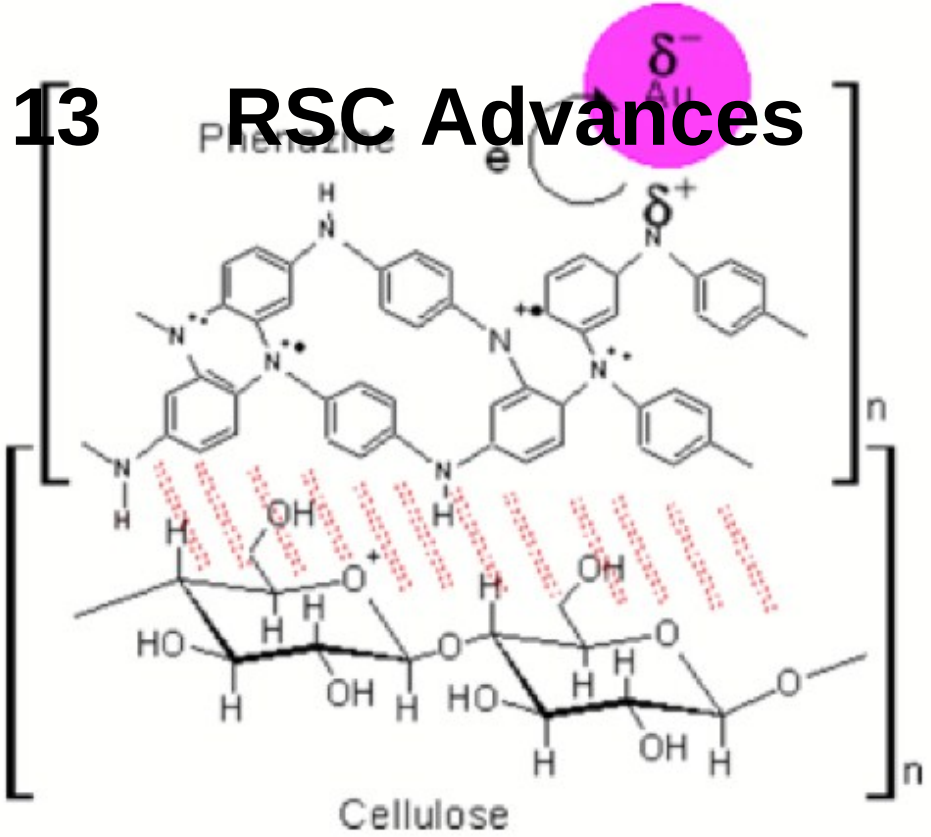

EFM